International Journal of Biological Macromolecules 159 (2020) 877–885

Contents lists available at ScienceDirect

International Journal of Biological Macromolecules

journal homepage: http://www.elsevier.com/locate/ijbiomac

Characterization of active/binding site residues of peptidyl-tRNA hydrolase using biophysical and computational studies

Rajkumar Kulandaisamy [a], Tushar Kushwaha [a], Vikas Kumar [a], Soumya De [b], Saroj Kumar [a], Santosh Kumar Upadhyay [c], Manoj Kumar [a], Krishna K. Inampudi [a,*]

[a] Department of Biophysics, All India Institute of Medical Sciences, New Delhi 110029, India
[b] School of Bio Science, Indian Institute of Technology, Kharagpur, West Bengal 721302, India
[c] CSIR-Institute of Genomics & Integrative Biology, New Delhi 110025, India

ARTICLE INFO

Article history:
Received 10 December 2019
Received in revised form 9 April 2020
Accepted 17 May 2020
Available online 20 May 2020

Keywords:
Mycobacterium tuberculosis (*M. tb*)
Escherichia coli (*E. coli*)
Peptidyl tRNA
Peptidyl tRNA hydrolase (PtH)
Peptidyl tRNA analogue
Isothermal titration calorimetry (ITC)
Fourier transform infra-red (FTIR) spectroscopy
Circular dichroism (CD) spectroscopy and modelling studies

ABSTRACT

All mRNAs cannot be translated into full-length proteins due to ribosome-stalling that leads to release of peptidyl-tRNA which can be lethal for bacterial survival. The enzyme peptidyl-tRNA hydrolase (PtH) hydrolyses the ester bond between nascent peptide and tRNA of peptidyl-tRNA and rescues the cells from toxicity. PtH is an essential enzyme in bacteria and inhibiting this crucial enzyme can serve to combat bacterial diseases. But due to lack of understanding about the catalytic mechanism of PtH, its inhibitors have not been developed. In this work, we have carried out the binding studies of *M. tuberculosis* and *E. coli* PtH with the peptidyl-tRNA analogue (puromycin) using ITC, FTIR, CD experiments followed by docking and MD simulations to identify the potential active site residues that would help to design PtH inhibitors. Binding studies of puromycin with both PtH by ITC experiments demonstrate similar thermodynamic parameters and three fold difference in their K_D. CD and FTIR studies detected changes in secondary structure composition of PtH in the presence of puromycin with different degree of perturbation. Though interactions with puromycin are conserved in both proteins, modelling studies revealed that water mediated interactions in *M. tb*-PtH resulting in higher affinity to puromycin.

1. Introduction

Bacterial translation machinery is one of the most exploited areas targeted by antibiotics. During the protein translation process, ~10% ribosomes get stalled along with peptidyl-tRNA due to truncated mRNA, scarcity of amino acids or aminoacyl-tRNAs, short ORF or minigenes expression [1–6]. The peptidyl-tRNA are released from ribosomes with the help of translation factors such as RRF, EFG, RF3, IF1, IF2, RelA or tmRNA [7]. The free peptidyl-tRNA could be lethal to the cells if peptidyl-tRNA hydrolase (PtH) enzyme does not hydrolyse the ester bond between tRNA and peptide [8–10]. PtH is a ubiquitous enzyme in the living system. Knock out study of PtH in yeast cells does not affect its survival [11] but it has been established as an essential protein for bacterial survival [12]. Also, there is significant structural differences between bacterial (PtH1) and eukaryotic (PtH2) PtH. Hence, PtH is an established drug target against bacterial pathogens [13,14]. However, there is complete lack of PtH inhibitor, primarily due to poor understanding of the structural basis of PtH activity. Though several structures of native PtH are available [14–18], active/binding site residues have been identified mainly by biochemical studies due to absence of structural complex of PtH with any inhibitor or substrate. Site directed mutagenesis of *E. coli* PtH have identified residues Asn10, His20, Asn68, Asp93 and Asn114 to be important for enzymatic function [19,20]. NMR studies of *E. coli* PtH with its minimal substrate analogue (3′-(L-[*N*,*N*-diacetyl-lysinyl) amino-3′-deoxyadenosine) have recognised additional residues like Gly111, Asn114, Leu116, Lys117, Gly147, Phe148 and Val149 forming the binding pocket [21]. The active site of PtH is associated with peptide binding as well as tRNA binding [22]. NMR studies of *E. coli*-PtH with an RNA mimic containing the acceptor and TψC stems has revealed several residues (Asn10, His20, Phe66, Met67, Asn68, Asp93, and His113, Asn114) important for tRNA recognition [19–23]. Mutagenesis and NMR studies from *Vibrio chloreae* PtH has also identified a set of residues (Asp14, His24, Asp97 and Asn118) involved in the enzymatic action [18].

* Corresponding author at: Department of Biophysics, All India Institute of Medical Sciences, New Delhi 110 029, India.
E-mail address: krishna.inampudi@aiims.edu (K.K. Inampudi).

https://doi.org/10.1016/j.ijbiomac.2020.05.133
0141-8130/

However, knowledge about active/binding site residues of *M. tb*-PtH is deficient. Only one crystal structure of *M. tb*-PtH has been reported [PDB:2Z2I] [24]. However, this does not provide any information about its active site due to absence of any ligand in the structure. Since the PtH is an attractive drug target for anti-TB drugs, its binding site information will help to design inhibitors against *M. tb*-PtH. Bal et al., have identified few important residues in the *M. tb* PtH catalytic site by site directed mutagenesis experiments [25]. Though there are many biochemical and structural studies, there is still an ambiguity in the binding residues and catalytic mechanism of the PtH. Till date there are no reported inhibitors against PtH due to the lack of understanding about its catalytic mechanism. A suitable starting point to design PtH inhibitors is to identify and characterize the binding site residues of *M. tb*-PtH. This would give impetus to rational design of PtH specific potent inhibitors.

In this work, we have carried out the binding studies of *M. tb*-PtH with puromycin, one of the peptidyl tRNA analogue, using ITC experiment followed by biophysical (CD, FTIR) and computational (docking and MD simulations) studies to identify its potential active site residues. Puromycin is a known closest structural analogue of PtH substrate which mimics 3′-end A76 aminoacyl tRNA and it has an ester bond between amino acid and nucleotide (Fig. 1). This ester bond between 3′ amino group of the ribose sugar and amino acid in puromycin makes it a more suitable substrate mimic of PtH. Similar studies were carried out with *E. coli* PtH to find the similarity and differences in binding of puromycin. This also helped to validate the data. Binding affinity (K_D) of puromycin was obtained to be greater for *M. tb*-PtH than *E. coli* PtH. The secondary structure of client protein was changed during interaction with puromycin confirmed by FTIR and Induced Circular dichroism (ICD) spectroscopic experiments. Modelling studies demonstrate that the binding site is dominated by the hydrophobic residues in both the proteins and a water mediated interaction has significant contribution in ligand binding in case of *M. tb*-PtH compared to *E. coli* PtH. These observations further have to be experimentally established by site directed mutagenesis studies which can guide to design the *M. tb* PtH specific inhibitors.

2. Materials and methods

2.1. Chemicals and reagents

Synthetic oligonucleotide primers were purchased from Integrated DNA Technologies, India. Ligation Independent Cloning (LIC) kit was purchased from Thermo Scientific, India. Puromycin was purchased from Biobasic Inc., Canada. All other chemicals and reagents used in the experiment are molecular biology reagent grade.

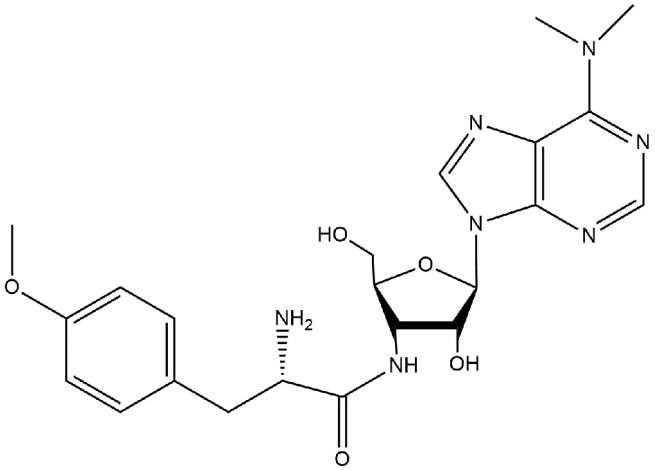

Fig. 1. Chemical Structure of Puromycin.

2.2. Cloning

Escherichia coli K12 strain genomic DNA was extracted by protocol established earlier [26]. *E. coli* Peptidyl tRNA hydrolase (PtH) gene was amplified by PCR using *E. coli* genomic DNA as a template and designed primers (5'-AGAAGGAGATATAACTATGGTGACATTAAATTGATTGTCG-3′ (forward) and (5'-GTGGTGGTGATGGTGATGGCCTTGCGCTTTAAAGGC GTGCA-3′ (reverse). Similarly, *M. tb*-PtH was also amplified by PCR using *Mycobacterium tuberculosis* H37Rv strain genomic DNA (received from Dr. Krishna Mohan's lab, THSTI, Haryana, India) and primers 5'-AGAAGGAGATATAACTATGGCCGAGCCGTTGCTCGTG-3′ (forward) and 5'-GTGGTGGTGATGGTGATGGCCCCAGGCGTGGACGCGGTT-3′ (reverse). The insert containing *M. tb*-PtH and *E. coli* PtH were ligated into pLATE31 vector that is having C-terminal 6-histidine tag. PCR amplified product of *M. tb* and *E. coli* PtH is shown in Fig. S1A & S1B. The clones were confirmed by DNA sequencing.

2.3. Expression and purification of E. coli PtH and M. tb PtH

For protein production, *E. coli* BL21(DE3) strain was transformed with plasmids encoding *M. tb*-PtH and *E. coli* PtH insert separately. Transformed colonies containing *M. tb*-PtH and *E. coli* PtH were inoculated in small culture and further grown in 1L LB media at 37 °C. 1 mM IPTG (Isopropyl β-d-1-thiogalactopyranoside) was added in growing cells at an OD $A_{600nm} = 0.6$ and further grown for 18 h at the same temperature. Cells were harvested at 7000 rpm for 10 min and resuspended in lysis buffer containing 50 mM sodium phosphate, 300 mM NaCl pH 8.0. After sonication, the cell lysate was centrifuged at 13000 rpm for 45 min and supernatant was loaded onto a Ni-NTA affinity column (GE Healthcare). PtH proteins were eluted with a linear gradient of lysis buffer containing 250 mM imidazole. Eluted fractions of *E. coli* and *M. tb* proteins were confirmed by 13% SDS-PAGE (Fig. S2A & B). Fractions containing PtH proteins were concentrated and loaded onto a Superdex 26/600 (200 pg) fast flow (GE Healthcare) column equilibrated with buffer containing 50 mM sodium phosphate, 50 mM NaCl, pH 7.5 (Fig. S3A & B). Eluted fractions containing PtH proteins were confirmed by 13% SDS-PAGE and concentrated with 10 kDa cutoff centricon (Amicon Ultra, Merck Millipore). The proteins were used immediately or stored at −80 °C prior to further use.

2.4. Isothermal titration calorimetric (ITC)

Isothermal Titration Calorimetry (ITC) experiments were carried out to get information about binding parameters of puromycin with *M. tb*-PtH and *E. coli* PtH. All the ITC experiments were carried out in buffer containing 50 mM sodium phosphate (pH 7.5), 50 mM NaCl using PEAQ-ITC microcalorimeter (Malvern Panalytical) at 298 K. Before performing ITC experiment, samples were filtered and dialysed. The titration cell was filled with *M. tb* PtH or *E. coli* PtH with the concentrations of 200 μM and titrated with syringe containing 4 mM puromycin. In each ITC experiment, total 13 injections containing 3 μL aliquots of puromycin were titrated into cell containing *M. tb*-PtH or *E. coli* PtH. The thermodynamic parameters were determined by fitting to a one-site binding model.

2.5. FTIR spectroscopy measurements

The protein sample (4 μL of 200 μM) was kept on the Attenuated Total Reflection (ATR). Fourier Transform Infra-Red (FTIR) measurement was done at 4 cm^{-1} spectral resolution on a Bruker Vertex 27 instrument equipped with DTGS detector. All experiments on FTIR spectrometer were performed by OPUS software at room temperature. In each experiment, the buffer single beam spectrum of 100 scans was recorded as a background spectrum. Thereafter, protein sample was recorded in the absorption mode with the same scans. The instrument was continuously purged with N_2 gas. Absorption spectra were

presented after baseline correction and 4 cm^{-1} smoothing. The processing of FTIR spectra was done using MATLAB (Mathworks Inc) program Kinetics [27,28]. The water vapour contributions in all spectra were verified by observing the spectral features above 1750 cm^{-1}. In the Fig. 4, all the spectra were normalized to equal band amplitudes.

2.6. Circular dichroism (CD) measurements

The CD spectra of the *E. coli* and *M. tb* PtH protein (20uM) with the puromycin, using different concentration (1:0, 1:1, 1:2, 1:3, 1:5, 1:10, 1:15, 1:20, 1:25, and 1:30 ratio) at 25 °C were acquired on a Jasco spectro polarimeter (Model J-1500). The spectra were obtained, using the spectro manager software which is thermostatically controlled by cell holder attached with the Jasco PTC-423S/15 peltier with a precision of ±0.1 °C. The reference sample of CD spectrum signal containing buffer 50 mM NaH_2PO_4 buffer, 50 mM NaCl pH 7.5 was subtracted. The spectra were recorded in the range of far-UV region (200–250 nm) using a quartz cell with a path length of 0.1 cm, a response time of 1 s, a scan speed of 20 nm/min and bandwidth of 0.5 nm and each spectrum is the average of three scans. The CD data were converted into the concentration-independent parameter, mean residue ellipticity [θ] (deg cm^2 $dmol^{-1}$), using the formula,

$$[\theta]_\lambda = M_o\, \theta_\lambda / 10 * cl]$$

θ_λ is the observed ellipticity in millidegrees, M_o is the mean residue weight of the protein, c is concentration in mg ml^{-1} and l is the path length of the cell in centimetres [29].

2.7. Molecular docking and MD simulation studies

Crystal structure of *M. tb*-PtH [PDB: 2Z2I] [24] and *E. coli* PtH [PDB: 2PTH] [19] were taken and only three solvent molecules in potential binding pocket were removed while retaining the rest of the solvent molecules. Each of the two protein structures was energy minimized to remove any van der Waals clashes and to optimize the interactions between their atoms. Energy minimized structures were used as receptor model for docking studies with puromycin. Binding site in *E. coli* PtH for docking studies were defined by the residues reported to be interacting with substrate/analogue. These include Asn10, Tyr15, His20, Phe66, Asn68, Asp93, Asn114 (identified by site directed mutagenesis/biochemical studies) [19,20,22,30,31] and Ala18, Thr20, Asp95, Glu96 (identified by NMR studies) [18, 21 and unpublished data]. Binding site in *M. tb*-PtH were defined over the putative binding pocket surrounded by residues corresponding to above defined binding site residues in *E. coli* PtH. The crystal coordinates of ligand, puromycin, was taken from Protein Data Bank [PDB: 2DPT] [32] and energy minimized before docking. The minimized puromycin was docked in the defined potential binding pocket of *M. tb*-PtH using molecular docking program AutoDock 4.2.6 [33,34] with previously reported docking run parameters [35–37]. Total of top 50 potential solutions (docked poses) were saved and clustered (conformations with r.m.s deviation of less than 1.5 Å were clustered together). Docked conformation in the larger cluster having the lowest free energy of binding was considered. Docked poses were selected based on the above criteria and previous information about binding mode of purine ring in similar ligands with PtH. Similar approach was used for docking of puromycin with *E. coli* PtH. Selected docked conformation of puromycin in docked complex of *M. tb*-PtH was energy minimized and refined by molecular dynamics (MD) simulations. MD simulation was performed using GROMACS (version 2018.7) [38,39] with the help of GROMOS 54a7 [40] force field parameters similar to previous studies [41,42]. Each complex was solvated in a dodecahedron box extending to 10 Å from protein atoms in each direction using SPC216 water model [43]. Solvated complex was neutralized with counter ions and energy minimized by steepest decent algorithm with convergent criteria of less than 1000.0 kJ/mol/nm. The energy minimized solvated complex was equilibrated at 300 K for 100 ps under NVT condition followed by 100 ps under NPT condition. Berendsen coupling algorithm was used to regulate temperature while Parrinello-Rahman algorithm was to regulate pressure of the system. It was followed by production run for 200 ns under NPT condition. All the stage of simulation was performed under periodic boundary conditions using Leap Frog dynamics integrator and step size of 2 fs in the presence of LINCS harmonic constrains. Particle Mesh Ewald (PME) algorithm was to compute long range electrostatic interactions. Identical approach and parameters were used to refine the docked complex of puromycin with *E. coli* PtH.

3. Results and discussion

3.1. Binding studies of puromycin with M. tb-PtH and E. coli PtH using ITC

ITC experiments were carried out to measure the binding affinity and associated thermodynamic parameters of puromycin for both the PtH proteins. The binding isotherms of puromycin with titration into *M. tb*-PtH and *E. coli* PtH at 298 K are shown in Fig. 2A & B. The binding isotherm for both titrations fit well to a one site binding model indicating site-specific binding of puromycin with PtH. The dissociation constant (K_D) of puromycin for *M. tb*-PtH and *E. coli* PtH at 298 K was determined to be 275 μM and 819 μM, respectively. This study reveals that the binding of puromycin with *M. tb*-PtH is approximately 3-fold stronger (275 μM) than that of *E. coli* PtH (819 μM). Thermodynamic parameters also reveal that binding is entropy driven (Fig. 3A and B) which indicates the predominant role of hydrophobic forces between puromycin and PtH in their binding. It was also observed that binding of puromycin with *M. tb*-PtH is entropically more favourable ($T\Delta S = -17.1$ kcal/mol) than *E. coli* PtH ($T\Delta S = -11.0$ kcal/mol). However enthalpic penalty is also higher in case of puromycin binding to *M. tb*-PtH ($\Delta H = 12.2$ kcal/mol) than *E. coli* PtH ($\Delta H = 6.83$ kcal/mol). Net change in free energy (ΔG) is compromised due to the enthalpic penalty in both the cases but results in more negative ΔG (−4.86 kcal/mol) or higher affinity for *M. tb* than *E. coli* PtH (−4.21 kcal/mol).

3.2. Conformational changes in M. tb-PtH and E. coli PtH in the presence of puromycin

To get insight into the secondary structural changes of PtH protein in the presence of puromycin, FTIR spectroscopy studies were performed. Fig. 4A and B shows the amide I region (1700–1600 cm^{-1}) which has a main contribution from the stretching vibrations of C═O group from the protein backbone. Due to the different geometry and their hydrogen bond pattern in the different types of protein secondary structures, the amide I region gives different C═O stretching vibrations [27]. Each infrared absorbance spectrum of the protein sample was referenced against the buffer background. We further checked the quality of spectrum by getting a straight baseline in the 1900–1800 cm^{-1} spectral region. The overlapping infrared bands in the amide I region were resolved by the second derivative analysis. This process helped to identify the number of infrared bands with their position.

Fig. 4A represents the absorbance spectra of *M. tb*-PtH (black) and *M. tb*-PtH with ligand (green). We observed majorly 4 bands in *M. tb*-PtH. According to the literature [27,28,44–47], the band observed near 1699 cm^{-1} was assigned to β sheets/turn, near 1682 cm^{-1} to loop/random coil, near 1649 cm^{-1} to α-helices/random coil and the band near 1636 cm^{-1} to β sheets conformations. We have observed 6 bands in the presence of ligand that β sheets/turn at 1699 cm^{-1} shifted to 1694 cm^{-1} while α-helices bands at 1649 cm^{-1} split at 1659 and 1650 cm^{-1}; also, β sheets conformations at 1636 cm^{-1} divided into 1640 and 1631 cm^{-1}. This indicates the secondary structure changes upon ligand binding and the protein is in more flexible conformation. The band observed near 1617 cm^{-1} arises from the ligand. Similarly, Fig. 4B shows the absorbance spectra of *E. coli* PtH (black) and *E. coli*

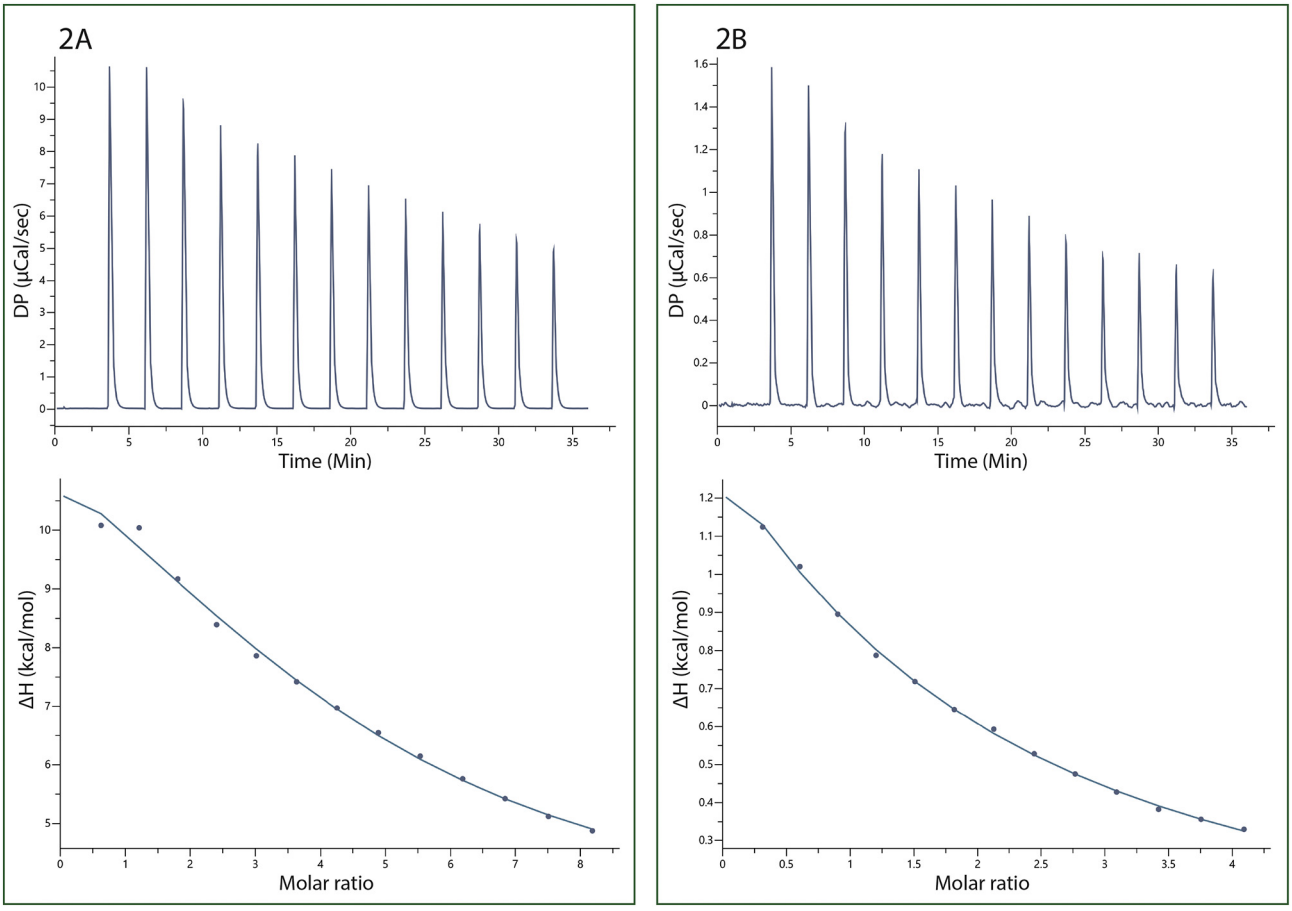

Fig. 2. Isothermal calorimetric titration (ITC) profiles (thermogram) of puromycin binding with **[A]** *M. tb*-PtH and **[B]** *E. coli* PtH.

PtH with ligand (green). The bands in *E. coli* PtH are observed near 1690 cm^{-1} to β sheets/turn, near 1676 cm^{-1} to random coils, 1656 cm^{-1} to α-helices and near 1637 cm^{-1} to β sheets. The secondary structural changes were observed upon ligand binding. In *E. coli* PtH with ligand, the bands are perturbed and the β sheets/turn changed to 1694 cm^{-1}, α-helices to 1654 cm^{-1} as well as the two bands arises near 1640 and 1633 cm^{-1} are the contribution of β sheets. The band observed at 1616 cm^{-1} is from the ligand.

In both *M. tb*-PtH and *E. coli* PtH proteins, conformational changes were observed upon ligand binding. In both the cases, the band near

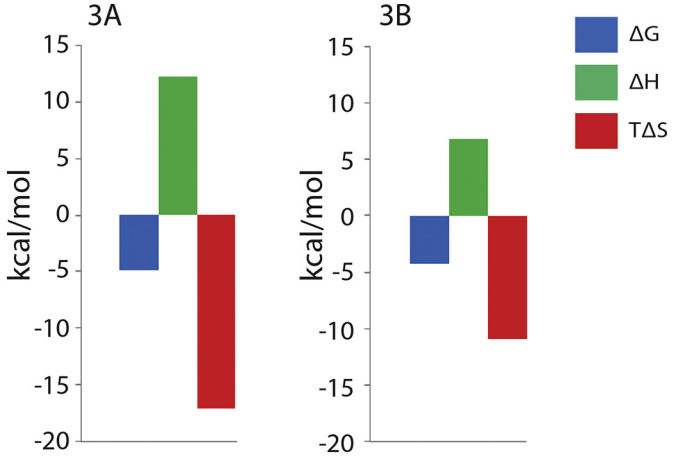

Fig. 3. ITC signature profile during binding of puromycin with **[A]** *M. tb*-PtH and **[B]** *E. coli* PtH.

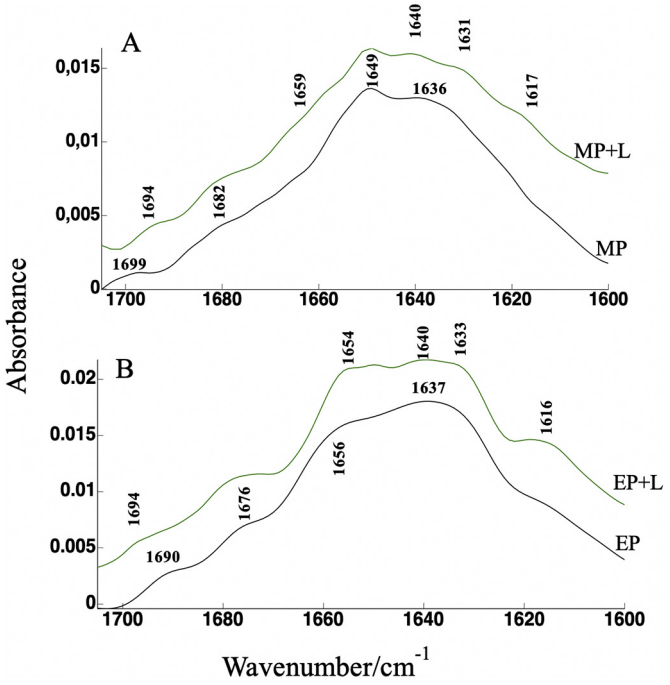

Fig. 4. Infra-Red (IR) absorbance spectra of **[A]** *M. tb* and **[B]** *E. coli* PtH with puromycin. Black and green lines correspond to PtH and PtH with puromycin, respectively.

1636/1637 cm^{-1} in the native protein changed into two bands near 1640 and 1631/1633 cm^{-1} in the presence of ligand indicating that interaction between them reflects the flexibility or alteration of the protein. Apart from the β-sheets, the band near 1640 cm^{-1} and 1630 cm^{-1} may also arise due to the presence of random coil and unstructured regions, respectively [44,48]. In the case of *E. coli* PtH, we observed an additional band near 1648 cm^{-1} in the presence of ligand indicating either ligand binding and/or the presence of random coil conformation. These changes reflect that the ligand binding leads more flexible regions in the protein. However, differences in the spectra (Fig. 4) of both proteins in the presence of the ligand highlight the differences in the ligand binding behaviour of puromycin to both the PtHs. This is in conformity with our ITC results where the entropic and enthalpic contributions of ligand binding are significantly different in both the cases (Figs. 2 and 3).

3.3. Secondary structure changes in *M. tb*-PtH and *E. coli* PtH in the presence of Puromycin

Circular dichroism (CD) provides the structural information about the bonds and structures by its chirality. When a ligand binds to the target protein, it induces the protein CD spectrum by electron rearrangements and can be used to study the binding of ligands molecules to the proteins. Here, our CD experiments shown Fig. 5A, the absorbance spectra of *M. tb* PtH (red) and induced absorbance CD spectra of *M. tb* PtH with different concentrations of the ligand (different colour). The perturbation of induced CD spectrum with increasing magnitude of the ligand indicating the one binding mode between the protein and ligand [49] that is corroborating with the ITC stoichiometric results. In the CD spectra, we have observed two distinct changes upon the ligand binding, the overall absorption decreased as well as the shape of the band were perturbed. The negative absorption of the band at 208 nm (π to π* transitions) decreased in comparison to the band at 222 nm (n to π* transitions) as well as the β sheets perturbation were also observed [50–52]. Fig. 5B, shows the absorbance spectra of *E. coli* PtH (red) and with the ligand (different colour), respectively. Here we observed the similar changes i. e perturbation of α- helices as well as in the β sheets. Also, we have observed that the distinct decrease in the 208 nm and 215 nm (n to π* transitions) band in comparison to the 222 nm, which are indicative of the flexible confirmation upon the binding [50–52], and induced CD spectra pattern is slightly different from the *M. tb*-PtH-puromycin complex. The change in absorption as well as different protein secondary structural changes in complex with the puromycin indeed support the differential ligand binding pattern and also corroborate with the ITC and FTIR studies.

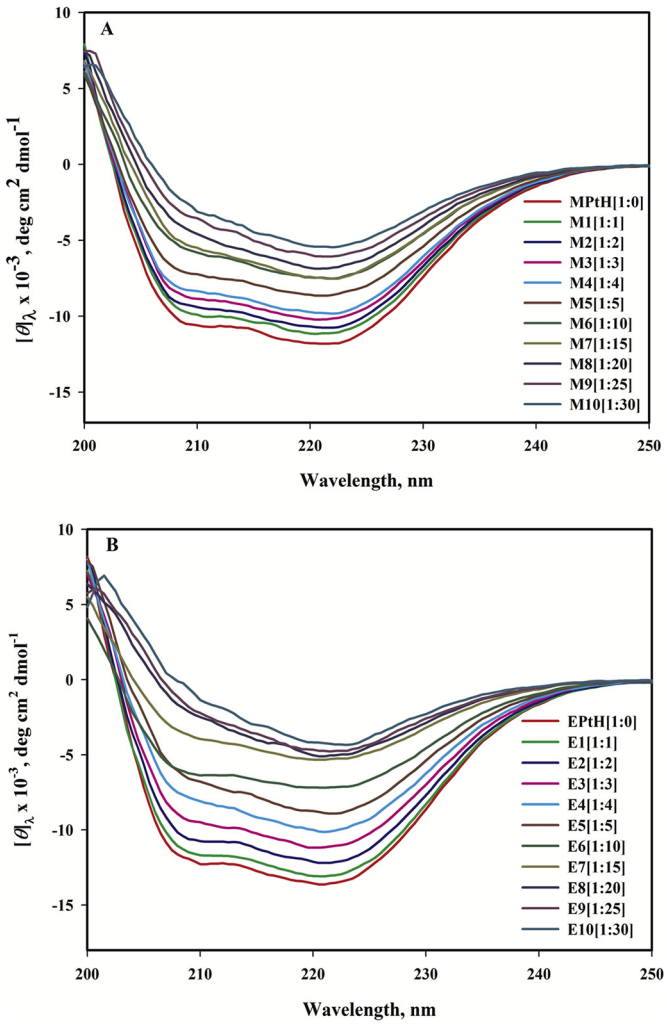

Fig. 5. CD spectrum signal of **[A]** *M. tb* and **[B]** *E. coli* PtH protein with different ratio of puromycin.

3.4. Modelling studies of puromycin with *M. tb* PtH and *E. coli* PtH

Modelling studies indicates that the binding mode of puromycin with *M. tb*-PtH and *E. coli* PtH is very much similar (Fig. 6). Puromycin has similar interaction patterns in both the cases. Puromycin in both cases predominantly forms hydrophobic interactions with non-polar side chains forming the binding pocket (Figs. 6 & 7). Phenyl ring of puromycin forms aromatic interactions with Tyr17 and Tyr68 of *M. tb*-PtH while it forms aromatic interactions with corresponding residues, Tyr15 and Phe66, of *E. coli* PtH (Fig. 7). Additionally, it also interacts with side chain of Met69 of *M. tb*-PtH and Met67 of *E. coli* PtH, respectively. Purine ring and non-polar substituent at the ring of puromycin forms van der Waal's interactions with non-polar side chains of Leu97, Pro146 and Ala147 of *M. tb*-PtH while it form van der Waal's interactions with Leu95, Val145, Val146 and Val149 of *E. coli* PtH. In addition to predominant non-polar interactions between puromycin and PtH, couple of polar contacts also looks crucial. Puromycin forms hydrogen bonds with His22 and Asn116 of *M. tb*-PtH (Figs. 6A, 7A & 7C) while it forms hydrogen bond with His20 and Asn114 of *E. coli* PtH (Figs. 6B, 7B & 7D). However, these hydrogen bonds have been observed at more than 70% of MD trajectory in case of *M. tb*-PtH while they were retained at only bout 30% trajectory. Also, a water mediated interaction were observed with *M. tb*-PtH which was absent in *E. coli*-PtH. These interactions might be contributing to higher affinity of puromycin for *M. tb*-PtH compared to *E. coli* PtH.

MD trajectories of the complexes of puromycin with two PtH also shows the similar dynamic behaviour of complexes with some differences. The root mean square (r. m. s) deviation of puromycin complexed with *M. tb* PtH is slightly less than r. m. s deviation observed in case of *E. coli* PtH-puromycin complex though the r. m. s deviation of two proteins in the complex are almost same (Fig. 8A). Similarly, radius of gyration plot of two complexes shows that *M. tb* PtH-puromycin complex is a little more stable than *E. coli* PtH-puromycin complex (Fig. 8B). Also, r. m. s fluctuation of two proteins are very much similar (Fig. 8C). These observations clearly show that binding of puromycin with *M. tb* PtH is comparatively more stable than binding with *E. coli* PtH. This observation is in agreement with binding data obtained by ITC experiments and this also validates the modelling results.

Analysis of modelled complex of puromycin with *M. tb*-PtH and *E. coli* PtH clearly reveals that binding mode of puromycin with two proteins are almost identical. This is due to highly conserved nature of binding site residues. 13 of the 16 binding site residues are identical in two proteins while two residues are conservatively substituted (Fig. S4). It is also clear that puromycin has majorly hydrophobic interactions with two proteins while it forms only two hydrogen bond with both

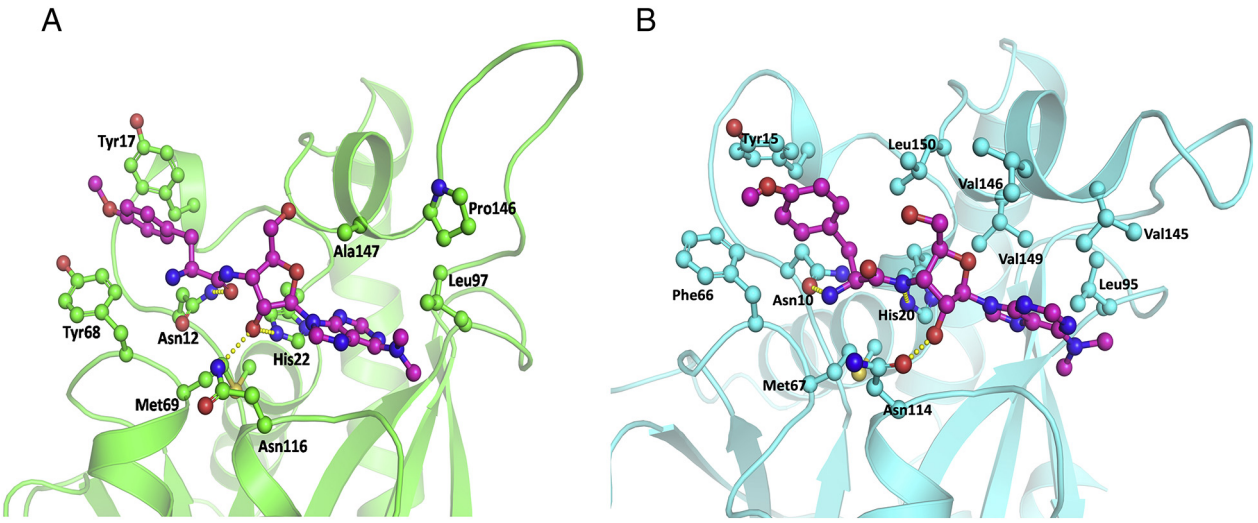

Fig. 6. Modelled complex of puromycin (ball & stick, magenta) with **[A]** PtH-*M. tb* (cartoon, green) and **[B]** PtH-*E. coli* (cartoon, cyan). Selected residues interacting with PtH are shown as ball and stick in respective colour.

the proteins (Fig. 7A and B). This observation is substantiated by the thermodynamic parameters observed in binding studies of puromycin with PtH during ITC experiment. ITC experiment found the higher contribution of entropic factor in binding of puromycin with PtH. The positive enthalpy observed in ITC experiment of puromycin binding with PtH might be due to predominant hydrophobic nature of the binding pocket.

(*M. tb* PtH – N12, Y17, H22, Y68, M69, N70, L97, G113, G114, H115, N116, P146, A147, V150, L151 &.

E. coli PtH – N10, Y15, A16, T18, H20, F66, M67, N68, D93, L95, G111, G112, H113, N114, V145, V146, V149, L150).

Additionally, the newly identified residue, Asp93, of *E. coli* PtH found to interact with puromycin by NMR experiment (unpublished data) is having interactions in *E. coli* PtH-puromycin modelled complex. This further endorses the *in silico* studies of ligand binding with PtH.

Majority of the residues of PtH implicated to be directly interacting with puromycin by modelling studies are present in the loop region which are less organised or existing in random conformation. Binding of puromycin with these residues might easily perturb their secondary structure conformation. This observation of modelling studies is corroborated by spectroscopy studies of PtH in the presence of puromycin. FTIR as well as CD spectroscopy studies show the marked perturbation

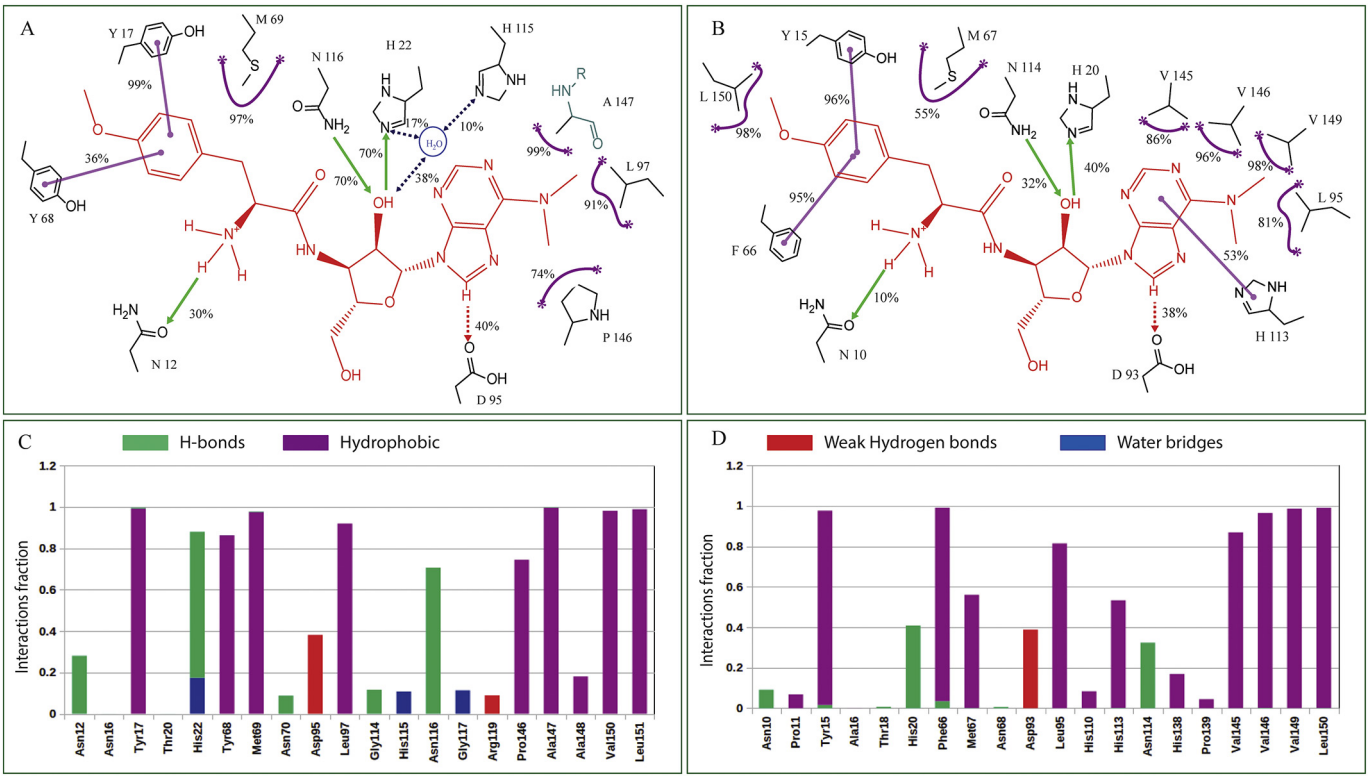

Fig. 7. Interactions observed during MD simulation of modelled complex of puromycin with (**A** & **C**) *M. tb*-PtH and (**B** & **D**) *E. coli* PtH. Interactions are shown in panel **[A]** & **[B]** through arrows in terms of percentage of the time observed during MD simulation while interactions are shown in panel **[C]** & **[D]** through rectangular bars in terms of fraction.

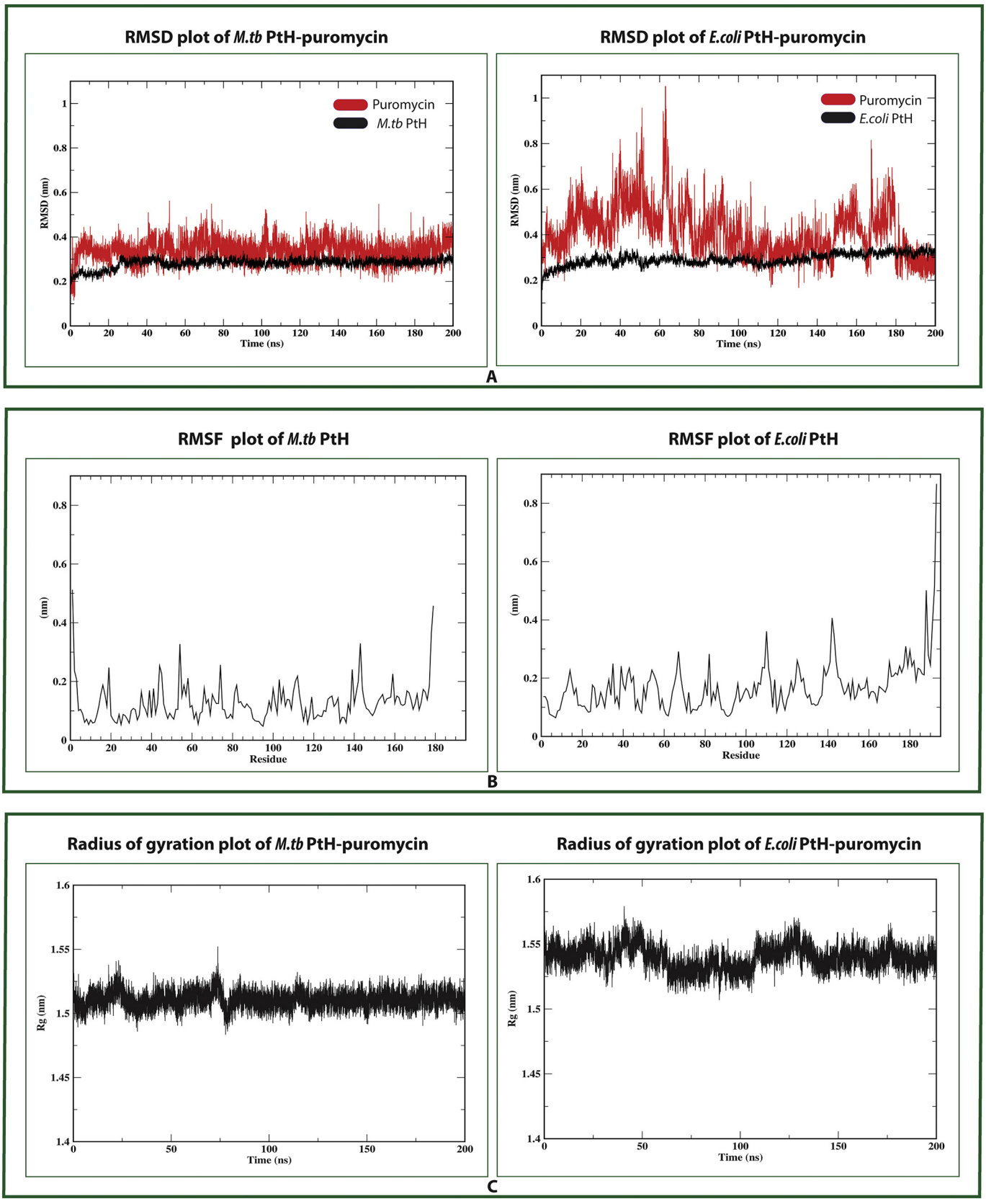

Fig. 8. Plots of MD trajectory of modelled complex of puromycin with PtH-*M. tb* (left panel) and PtH-*E. coli* (right panel). **[A]** r. m. s deviation plot, **[B]** r. m. s fluctuation plot **[C]** radius of gyration plot.

in secondary structure conformation of the protein in the presence of puromycin (Fig. 4A & B). These observations also validate the binding mode of puromycin with PtH in modelled complex. Hence this study helped to identify the key residues in the active site of *M. tb* PtH and this information will guide the design of its potent inhibitors.

From our studies, we have demonstrated that the binding affinity (K_D) of puromycin for *M. tb*-PtH and *E. coli* PtH using ITC experiment and the binding was also confirmed by FTIR and CD experiments. It is also interesting to know how two homologous proteins (*M. tb* & *E. coli*) are responding to their substrate analogue and a comparison will help to understand the differences/similarities of potencies of *M. tb* PtH specific inhibitors during cell-based screening study which is available only in *E. coli* model (in *E. coli* AA7852 temperature sensitive strain). And this combined study would also be helpful to validate the importance of identified residues by site directed mutagenesis studies which would be continuation of this work. Using FTIR and CD experiments, we have shown that the secondary structure of client protein changes during interaction with puromycin. Modelling studies demonstrate that water mediated interaction has significant contribution in ligand binding in case of *M. tb* PtH compared to *E. coli* PtH. These observations further have to be experimentally established in *E. coli* AA7852 cells and are in progress in our lab.

4. Conclusion

The binding affinity of peptidyl tRNA mimic, puromycin, is about 3-fold higher for *M. tb*-PtH (275 μM) than *E. coli* PtH (819 μM). Thermodynamic parameters of puromycin binding with two PtH obtained from ITC experiment reveals that binding is entropy driven. Though the binding site of two PtH is highly conserved but binding affinity of puromycin for two proteins are significantly different. FTIR and CD experiments also substantiate the differential binding as the changes observed in secondary structure of two PtH was not very similar. Furthermore, conformational changes are observed in both PtH upon ligand binding indicates that the secondary structure changes in the protein resulting in more flexible conformation or ligand induced alteration in the protein. In case of *M. tb*-PtH, conformational changes were observed for α-helices and β sheets in the presence of puromycin. While in case of *E. coli* PtH, conformational perturbation was observed for β sheets/turn, α-helices and random coils. Modelling studies also endorse the differential interactions of puromycin with two PtH supporting the FTIR, CD experiments and binding affinities obtained by ITC studies. These studies provides important information about binding site of PtH substrate mimic and could help in design of potent inhibitors of *M. tb*-PtH which is an attractive novel drug target for anti-TB drug development.

Supplementary data to this article can be found online at https://doi.org/10.1016/j.ijbiomac.2020.05.133.

Author's contributions

RK & KKI planned and designed the experiments. RK performed all the experiments. SKU and SK helped with the ITC, FTIR experiments, respectively. RK,TK performed the docking and simulation experiments respectively with MK. SD and VK thoroughly proof read and provided valuable inputs for the improvement of the manuscript. RK, MK & KKI wrote the manuscript taking inputs from all the authors.

Declaration of competing interest

The authors declare no conflict of interests.

Acknowledgements

We are grateful for providing the instrument facility from Department of Biophysics, AIIMS, New Delhi-110029. We also thank Dr. Kapil Dev for FTIR experiments from Jamia Millia Islamia University and CSIR-IGIB, New Delhi, India for Isothermal titration calorimetry (ITC) experiments and KK thanks to Dr. Krishna Mohan's, THSTI, Haryana for kindly providing the *Mycobacterium tuberculosis* H37Rv genomic DNA. This work was financially supported by grants from DST-SERB extramural and AIIMS Intramural Projects.

Ethical approval

This article does not involve any study with human participants or animals to be performed by any of the authors.

References

[1] J.R. Menninger, C. Walker, P.F. Tan, A.G. Atherly, Studies on the metabolic role of peptidyl-tRNA hydrolase: I. Properties of a mutant *E. coli* with temperature-sensitive peptidyl-tRNA hydrolase, MGG Molecular & General Genetics 121 (1973) 307–324, https://doi.org/10.1007/BF00433230.
[2] A.B. Caplan, J.R. Menninger, Tests of the ribosomal editing hypothesis: amino acid starvation differentially enhances the dissociation of peptidyl-tRNA from the ribosome, J. Mol. Biol. 134 (3) (1979 Nov 5) 621–637 (n.d.).
[3] Heurgué-Hamard, V., Karimi, R., Mora, L., MacDougall, J., Leboeuf, C., Grentzmann, G., … & Buckingham, R. H. (1998). Ribosome release factor RF4 and termination factor RF3 are involved in dissociation of peptidyl-tRNA from the ribosome. EMBO J., 17 (3), 808–816., (n.d.).
[4] R. Karimi, M.Y. Pavlov, V. Heurgué-Hamard, R.H. Buckingham, M. Ehrenberg, Initiation factors IF1 and IF2 synergistically remove peptidyl-tRNAs with short polypeptides from the P-site of translating *Escherichia coli* ribosomes, J. Mol. Biol. 281 (2) (1998 Aug 14) 241–252 (n.d.).
[5] L.R. Cruz-Vera, M.A. Magos-Castro, E. Zamora-Romo, G. Guarneros, Ribosome stalling and peptidyl-tRNA drop-off during translational delay at AGA codons, Nucleic Acids Res. 32 (15) (2004) 4462–4468 (n.d.).
[6] S. Vivanco-Domínguez, J. Bueno-Martínez, G. León-Avila, N. Iwakura, A. Kaji, H. Kaji, G. Guarneros, Protein synthesis factors (RF1, RF2, RF3, RRF, and tmRNA) and peptidyl-tRNA hydrolase rescue stalled ribosomes at sense codons, J. Mol. Biol. 417 (5) (2012 Apr 13) 425–439 (n.d.).
[7] N.S. Singh, U. Varshney, A physiological connection between tmRNA and peptidyl-tRNA hydrolase functions in *Escherichia coli*, Nucleic Acids Res. 32 (20) (2004) 6028–6037 (n.d.).
[8] G. Das, U. Varshney, Peptidyl-tRNA hydrolase and its critical role in protein biosynthesis, Microbiology 152 (8) (2006 Aug 1) 2191–2195 (n.d.).
[9] J.R. Menninger, Accumulation of peptidyl tRNA is lethal to *Escherichia coli*, J. Bacteriol. 137 (1) (1979 Jan 1) 694–696 (n.d.).
[10] K. Ito, H. Qi, Y. Shimizu, R. Murakami, K.I. Miura, T. Ueda, T. Uchiumi, Crystallization and preliminary X-ray analysis of peptidyl-tRNA hydrolase from *Escherichia coli* in complex with the acceptor-TΨC domain of tRNA, Acta Crystallogr. Sect. F: Struct. Biol. Cryst. Commun. 67 (12) (2011) 1566–1569 (n.d.).
[11] G. Rosas-Sandoval, A. Ambrogelly, J. Rinehart, D. Wei, L.R. Cruz-Vera, D.E. Graham, ... D Söll, Orthologs of a novel archaeal and of the bacterial peptidyl-tRNA hydrolase are nonessential in yeast, Proceedings of the National Academy of Sciences 99 (26) (2002) 16707–16712 (n.d.).
[12] Valerie Heurgué-Hamard, Liliana Mora, G. Guarneros, R.H. Buckingham, The growth defect in *Escherichia coli* deficient in peptidyl-tRNA hydrolase is due to starvation for Lys-tRNA (Lys), EMBO J. 15 (11) (1996) 2826–2833 (n.d.).
[13] R.L. McFeeters, Recent antimicrobial developments targeting peptidyl-tRNA hydrolases, JSM Biotech Biomed Eng 1 (2013) 1006 (n.d.).
[14] S. Sharma, S. Kaushik, M. Sinha, G.S. Kushwaha, A. Singh, J. Sikarwar, A. Chaudhary, A. Gupta, P. Kaur, T.P. Singh, Structural and functional insights into peptidyl-tRNA hydrolase, Biochimica et Biophysica Acta (BBA)-Proteins and Proteomics 1844 (7) (2014 Jul 1) 1279–1288 (n.d.).
[15] V. Vandavasi, K. Taylor-Creel, R.L. McFeeters, L. Coates, H. McFeeters, Recombinant production, crystallization and X-ray crystallographic structure determination of peptidyl-tRNA hydrolase from *Salmonella typhimurium*, Acta Crystallographica Section F: Structural Biology Communications 70 (7) (2014) 872–877 (n.d.).
[16] Singh, A., Gautam, L., Sinha, M., Bhushan, A., Kaur, P., Sharma, S., & Singh, T. P. (2014). Crystal structure of peptidyl-tRNA hydrolase from a Gram-positive bacterium, *Streptococcus pyogenes* at 2.19 Å resolution shows the closed structure of the substrate-binding cleft. FEBS Open Bio, 4, 915–922., (n.d.).
[17] F. Zhang, Y. Song, L. Niu, M. Teng, X. Li, Crystal structure of *Staphylococcus aureus* peptidyl-tRNA hydrolase at a 2.25 Å resolution, Acta Biochim. Biophys. Sin. 47 (12) (2015) 1005–1010 (n.d.).
[18] Ashish Kabra, Salman Shahid, Ravi Kant Pal, Rahul Yadav, S.V.S. Rama Krishna Pulavarti, Anupam Jain, Sarita Tripathi, Ashish Arora, Unraveling the stereochemical and dynamic aspects of the catalytic site of bacterial peptidyl-tRNA hydrolase, RNA 23 (2) (2017) 202–216 (n.d.).
[19] E. Schmitt, Y. Mechulam, M. Fromant, P. Plateau, S. Blanquet, Crystal structure at 1.2 Å resolution and active site mapping of *Escherichia coli* peptidyl-tRNA hydrolase, EMBO J. 16 (15) (1997) 4760–4769 (n.d.).
[20] J.J. Goodall, G.J. Chen, M.G. Page, Essential role of histidine 20 in the catalytic mechanism of *Escherichia coli* peptidyl-tRNA hydrolase, Biochemistry 43 (15) (2004) 4583–4591 (n.d.).

[21] L. Giorgi, P. Plateau, G. O'Mahony, C. Aubard, M. Fromant, A. Thureau, M. Grøtli, S. Blanquet, F. Bontems, NMR-based substrate analogue docking to Escherichia coli peptidyl-tRNA hydrolase, J. Mol. Biol. 412 (4) (2011 Sep 30) 619–633 (n.d.).
[22] L. Giorgi, F. Bontems, M. Fromant, C. Aubard, S. Blanquet, P. Plateau, RNA-binding site of Escherichia coli peptidyl-tRNA hydrolase, J. Biol. Chem. 286 (45) (2011) 39585–39594 (n.d.).
[23] Kosuke Ito, Hao Qi, Yoshihiro Shimizu, Ryo Murakami, Kin-ichiro Miura, Takuya Ueda, Toshio Uchiumi, Crystallization and preliminary X-ray analysis of peptidyl-tRNA hydrolase from Escherichia coli in complex with the acceptor-TΨC domain of tRNA, Acta Crystallogr. Sect. F: Struct. Biol. Cryst. Commun. 67 (12) (2011) 1566–1569 (n.d.).
[24] M. Selvaraj, S. Roy, N.S. Singh, R. Sangeetha, U. Varshney, M. Vijayan, Structural plasticity and enzyme action: crystal structures of *Mycobacterium tuberculosis* peptidyl-tRNA hydrolase, J.Mol.Biol. 372 (2007) 186–193 (n.d.).
[25] N.C. Bal, H. Agrawal, A.K. Meher, A. Arora, Characterization of peptidyl-tRNA hydrolase encoded by open reading frame Rv1014c of *Mycobacterium tuberculosis* H37Rv, Biol. Chem. 388 (2007)https://doi.org/10.1515/BC.2007.057.
[26] E.D. Moore, A.N. Arnscheidt, A. Krüger, C. Strömpl, M. Mau, Simplified protocols for the preparation of genomic DNA from bacterial cultures, Molecular Microbial Ecology Manual 1 (1) (1999) 1–5 (n.d.).
[27] E. Goormaghtigh, V. Cabiaux, J.M. Ruysschaert, Secondary structure and dosage of soluble and membrane proteins by attenuated total reflection Fourier-transform infrared spectroscopy on hydrated films, Eur. J. Biochem. 193 (1990) 409–420 (n.d.).
[28] Valdivia AA, Barth A, Batista YR & Kumar S (2013) Characterization of recombinant antibodies for cancer therapy by infrared spectroscopy. Biologicals 41, 104–110., (n.d.).
[29] S.M. Kelly, T.J. Jess, N.C. Price, How to study proteins by circular dichroism, Biochim. Biophys. Acta 1751 (2) (2005) 119–139 (n.d.).
[30] Singh, A., Kumar, A., Gautam, L., Sharma, P., Sinha, M., Bhushan, A., ... & Singh, T. P. (2014). Structural and binding studies of peptidyl-tRNA hydrolase from *Pseudomonas aeruginosa* provide a platform for the structure-based inhibitor design against peptidyl-tRNA hydrolase. Biochem. J., 463(3), 329–337., (n.d.).
[31] S. Shahid, A. Kabra, S. Mundra, R.K. Pal, S. Tripathi, A. Jain, A. Arora, Role of methionine 71 in substrate recognition and structural integrity of bacterial peptidyl-tRNA hydrolase, Biochimica et Biophysica Acta (BBA) - Proteins and Proteomics 1866 (8) (2018) 865–874, https://doi.org/10.1016/j.bbapap.2018.05.002 (n.d.).
[32] Suto, K, Watanabe, K., Ueda, T., Fukai, S., Nureki, O., Tomita, K. (2006) Crystal structures of leucyl/phenylalanyl-tRNA-protein transferase and its complex with an aminoacyl-tRNA analog. EMBO J. 25: 5942–5950, (n.d.).
[33] G.M. Morris, R. Huey, W. Lindstrom, M.F. Sanner, R.K. Belew, D.S. Goodsell, A.J. Olson, Autodock4 and AutoDockTools4: automated docking with selective receptor flexiblity, J. Comput. Chem. 30 (2009) 2785–2791 (n.d.).
[34] G.M. Morris, D.S. Goodshell, R.S. Halliday, R. Huey, W.E. Hart, R.K. Belew, A.J. Olson, Automated docking using a Lamarckian genetic algorithm and empirical binding free energy function, J. Comput. Chem. 19 (1998) 1639–1662 (n.d.).
[35] G.S. Rao, M. Kumar, Structure-based design of a potent and selective small peptide inhibitor of Mycobacterium tuberculosis 6-hydroxymethyl-7, 8-dihydropteroate synthase: a computer modelling approach, Chem. Biol. Drug Des. 71 (2008) 540–545., (n.d.).
[36] R. Kumar, A.K. Singh, M. Kumar, S. Shekhar, N. Rai, P. Kaur, R. Parshad, S. Dey, Serum 5-LOX: a progressive protein marker for breast cancer and new approach for therapeutic target, Carcinogenesis 37 (2016) 912–917 (n.d.).
[37] G. Pandey, S. Bakhshi, M. Kumar, B. Thakur, P. Jain, P. Kaur, S.S. Chauhan, Prognostic and therapeutic relevance of cathepsin B in pediatric acute myeloid leukemia, Am. J. Cancer Res. 9 (2019) 2634–2649 (n.d.).
[38] M.J. Abraham, T. Murtola, R. Schulz, S. Páll, J.C. Smith, B. Hess, E. Lindahl, GROMACS: high performance molecular simulations through multi-level parallelism from laptops to supercomputers, SoftwareX 1–2 (2015) 19–25 (n.d.).
[39] H.J.C. Berendsen, D. van der Spoel, R. van Drunen, GROMACS: a message-passing parallel molecular dynamics implementation, Comput. Phys. Commun. 91 (1995) 43–56 (n.d.).
[40] N. Schmid, A.P. Eichenberger, A. Choutko, S. Riniker, M. Winger, A.E. Mark, W.F. van Gunsteren, Definition and testing of the GROMOS force-field versions 54A7 and 54B7, Eur. Biophys. J. 40 (2011) 843–856 (n.d.).
[41] P. Yadav, M. Kumar, R. Bansal, P. Kaur, A.S. Ethayathulla, Structure model of ferrochelatase from Salmonella typhi elucidating metalation mechanism, Int. J. Biol. Macromol. 127 (2019) 585–593 (n.d.).
[42] M.I. Khan, A.K. Gupta, D.R. Kumar, M. Kumar, A.S. Ethayathulla, G. Hariprasad, Molecular modeling of Gly80 and Ser80 variants of human group IID phospholipase A2 and their receptor complexes: potential basis for weight loss in chronic obstructive pulmonary disease, J. Mol. Model. 22 (2016) 232 (n.d.).
[43] D. van der Spoel, P.J. van Maaren, H.J.C. Berendsen, A systematic study of water models for molecular simulation: derivation of water models optimized for use with a reaction field, J. Chem. Phys. 108 (1998) 10220–10230 (n.d.).
[44] F. Zhang, et al., Molecular interactions of benzophenone UV filters with human serum albumin revealed by spectroscopic techniques and molecular modeling, J. Hazard. Mater. 263 (2013) 618–626 (n.d.).
[45] D.M. Byler, H. Susi, Examination of the secondary structure of proteins by deconvolved FTIR spectra, Biopolymers 25 (1986) 469e87 (n.d.).
[46] A. Barth, Infrared spectroscopy of proteins, Biochim. Biophys. Acta 1767 (2007) 1073e101 (n.d.).
[47] S. Kumar, A. Barth, Phosphoenolpyruvate and Mg2þ binding to pyruvate kinase monitored by infrared spectroscopy, Biophys. J. 98 (2010) 1931e40 (n.d.).
[48] V. Sharma, A. Srinivasan, A. Roychoudhury, K. Rani, M. Tyagi, K. Dev, F. Nikolajeff, S. Kumar, Characterization of protein extracts from different types of human teeth and insight in biomineralization, Sci. Rep. 9 (2019) 9314 (n.d.).
[49] A. Rodger, R. Marrington, D. Roper, S. Windsor, Circular dichroism spectroscopy for the study of protein-ligand interactions, Protein-Ligand Interactions, Humana Press 2005, pp. 343–363 , (n.d.).
[50] B. Ranjbar, P. Gill, Circular dichroism techniques: biomolecular and nanostructural analyses-a review, Chem. Biol. Drug Des. 74 (2) (2009) 101–120 (n.d.).
[51] R. Hussain, G. Siligardi, Characterisation of conformational and ligand binding properties of membrane proteins using synchrotron radiation circular dichroism (SRCD), The Next Generation in Membrane Protein Structure Determination, Springer, Cham. Chicago 2016, pp. 43–59 , (n.d.).
[52] G. Siligardi, C.S. Hughes, R. Hussain, Characterisation of sensor kinase by CD spectroscopy: golden rules and tips, Biochem. Soc. Trans. 46 (6) (2018) 1627–1642 (n.d.).